ETHzürich

Journal Article

Receiver function study of the Hellenic subduction zone: imaging crustal thickness variations and the oceanic Moho of the descending African lithosphere

Author(s):
Li, X.; Bock, G.; Vafidis, A.; Kind, R.; Harjes, H.P.; Hanka, W.; Wylegalla, K.; Meijde, M. van der; Yuan, X.

ETH Library

Receiver function study of the Hellenic subduction zone: imaging crustal thickness variations and the oceanic Moho of the descending African lithosphere

X. Li,[1] G. Bock,[1,]* A. Vafidis,[2] R. Kind,[1] H.-P. Harjes,[3] W. Hanka,[1] K. Wylegalla,[1] M. van der Meijde[4] and X. Yuan[1]

[1] *GeoForschungsZentrum Potsdam, Telegrafenberg,* 14473 *Potsdam, Germany. E-mail: li@gfz-potsdam.de*
[2] *Department of Mineral Resources Engineering, Technical University of Chania, Crete, Greece*
[3] *Institut für Geophysik, Ruhr-Univeristät Bochum,* 44780 *Bochum, Germany*
[4] *Institut für Geophysik, ETH Zürich,* 8096 *Zürich, Switzerland*

SUMMARY

We use data from recently installed broad-band seismographs on the islands of Crete, Gavdos, Santorini, Naxos and Samos in the Hellenic subduction zone to construct receiver function images of the crust and upper mantle from south of Crete into the Aegean Sea. The stations are equipped with STS-2 seismometers and they are operated by GFZ Potsdam, University of Chania and ETH Zürich. Teleseismic earthquakes recorded by these stations at epicentral distances between 35° and 95° have been used to calculate receiver functions. The receiver function method is a routinely used tool to detect crustal and upper-mantle discontinuities beneath a seismic station by isolating the *P*–*S* converted waves from the coda of the *P* wave. Converted *P*–*S* energy from the oceanic Moho of the subducted African Plate is clearly observed beneath Gavdos and Crete at a depth ranging from 44 to 69 km. This boundary continues to the north to nearly 100 km depth beneath Santorini island. Because of a lack of data the correlation of this phase is uncertain north of Santorini beneath the Aegean Sea. Moho depths were calculated from primary converted waves and multiply reflected waves between the Moho and the Earth's surface. Beneath southern and eastern Crete the Moho lies between 31 and 34 km depth. Beneath western and northern Crete the Moho is located at 32 and 39 km depth, respectively, and behaves as a reversed crust–mantle velocity contrast, possibly caused by hydration and serpentinization of the forearc mantle peridotite. The Moho beneath Gavdos island located south of Crete in the Libyan Sea is at 26 km depth, indicating that the crust south of the Crete microcontinent is also thinning towards the Mediterranean ridge. This makes it unlikely that part of the crust in Crete consists of accreted sediments transported there during the present-day subduction process which began approximately 15 Ma because the backstop, i.e. the boundary between the current accretionary wedge of the Mediterranean ridge and the Crete microcontinent, is located approximately 100 km south of Gavdos. A seismic boundary at 32 km depth beneath Santorini island probably marks the crustal base of the Crete microcontinent. A shallower seismic interface beneath Santorini at 20–25 km depth may mark the depth of the detachment between the Crete microcontinent and the overlying Aegean subplate. The Moho in the central and northern Aegean, at Naxos and Samos, is observed at 25 and 28 km depth, respectively. Assuming a stretching factor of 1.2–1.3, crustal thickness in the Aegean was 30–35 km at the inception of the extensional regime in the Middle Miocene.

Key words: Crete, crustal structure, Hellenic arc, receiver functions, subduction, Wadati–Benioff zone.

1 INTRODUCTION

The Hellenic arc is an arcuate feature extending from the Peloponnesos in the northwest to the island of Crete in the south (Fig. 1). It is

*Deceased (2002 November 6).

formed by the northward subduction of the African Plate under the Eurasian Plate. The convergence rate of the African and Eurasian Plate is low, of the order of 10 mm yr^{-1}. However, because of high deformation in the Aegean partly caused by the westward migration of the Anatolian subplate (Le Pichon *et al.* 1995) and the roll-back of the subducting African lithosphere, the relative displacement along
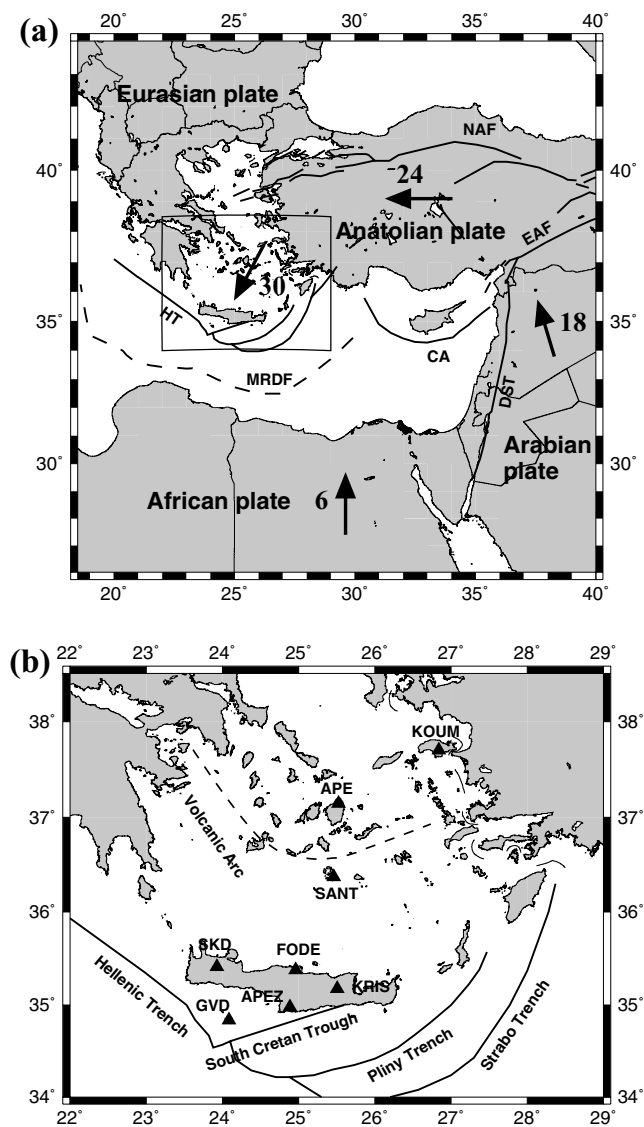
Figure 1. (a) Simplified tectonic map of the Eastern Mediterranean (CA = Cyprian arc; DST = Dead Sea Transform; EAF = East Anatolian Fault; HT = Hellenic Trench; MRDF = Mediterranean Ridge Deformation Front; NAF = North Anatolian Fault). Plate velocities are depicted by arrows, values in mm yr^{-1}, after McClusky *et al.* (2000). (b) Closeup view of the Hellenic arc system. Broad-band stations used in this study are shown by filled triangles.

the Hellenic arc is larger, of the order of 40 mm yr^{-1} (Reilinger *et al.* 1997; McClusky *et al.* 2000). Thus, the Hellenic arc and the Aegean move southward relative to stable Eurasia (Fig. 1a).

McKenzie (1972) and Jackson & McKenzie (1984) have introduced a plate tectonic model for the eastern Mediterranean (Fig. 1a), which explains significant regional features and which has been later confirmed by GPS measurements (Reilinger *et al.* 1997; McClusky *et al.* 2000). Resulting from the collision of the Arabian Plate with Eurasia, the Anatolian Plate is squeezed westward with an average rate of 24 mm yr^{-1} along the North Anatolian fault and 9 mm yr^{-1} along the East Anatolian fault, while the central and southern Aegean moves towards the SW at 30 mm yr^{-1} (McClusky *et al.* 2000). The extension of the Aegean explains the high convergence rate of 40–50 mm yr^{-1} along the Hellenic arc.

The convergent plate boundary marked by the Hellenic arc is characterized by high seismicity, with strong earthquakes up to

$M_s = 8.3$ at shallow depth in historic times, and a northward-dipping Wadati–Benioff zone (e.g. Papazachos & Kiratzi 1996; Papazachos 1999). As yet, a unified view on the details of the subduction process along the Hellenic arc has not been reached. It is not clear whether subduction begins in the area of the Hellenic trench (e.g. Jarrard 1986; Jackson 1994) or further south in an area of the furrow between the Mediterranean ridge and the African continental slope (e.g. Kastens 1991; von Huene 1997). The crust and the lithospheric mantle are strongly deformed in relation to the subduction process. Crustal images of western Crete derived from receiver function analysis have been interpreted to indicate that the oceanic crust–mantle boundary of the subducting oceanic plate can be traced at 40–60 km depth while the crust consists of a 15–20 km thick continental top layer overlying a fossil accretionary wedge (Knapmeyer & Harjes 2000).

On a larger scale, the subducted African Plate is seen at least down to 600 km depth by tomographic studies (Spakman *et al.* 1988; Wortel *et al.* 1990; Papazachos & Nolet 1997), while the seismicity stops at approximately 200 km depth (Papazachos *et al.* 2000). The Wadati–Benioff seismicity is diffuse, indicating a complicated structure of the Wadati–Benioff zone and the subduction processes (Knapmeyer 1999).

In this paper we use data from a network of broad-band stations in Crete, Gavdos and the Aegean to derive a receiver function image of the Hellenic subduction zone. We concentrate our study on obtaining reliable estimates of the crustal thickness and the depth of the descending African Plate. The results of the study suggest that crustal structure in Crete is very complex with a continental-type crust, and that the Moho of the subducting oceanic lithosphere can be reliably traced to approximately 100 km depth.

2 TELESEISMIC RECEIVER FUNCTION METHOD AND DATA

Teleseismic receiver functions are nowadays often used to determine crustal and upper-mantle discontinuities beneath a seismic station (Langston 1977; Owens *et al.* 1984; Li *et al.* 2000; Yuan *et al.* 2000). The receiver function method makes use of waves that are converted from *P* to *SV* at a seismic discontinuity beneath a receiver (Fig. 2). *P*–*S* converted waves are best observed at epicentral distances between 35° and 95° and they appear in the coda of *P*. The weak converted energy amounts to a few per cent of the *P*-wave energy. The converted phase can be displayed within the *P*-wave coda by means of rotating the three-component ZNE recording system into an LQT ray-based coordinate system, in which the L-component is in the direction of the incident *P* wave; the Q-component is perpendicular to the L-component and is positive away from the source; the T-component is the third component of the LQT right-hand system. The L component is dominated by the *P* wave, while the Q and T components contain mainly the converted *S*-wave energy (Fig. 2b). For horizontally layered homogeneous media, the converted *S*-wave energy is exclusively contained in the Q component. The presence of significant energy on the T component indicates laterally varying and/or anisotropic structure.

To eliminate the influence of the source and ray path, an equalization scheme is applied by deconvolving the Q- and T-component seismograms with the L-component seismogram. The resulting Q- and T-component data are named Q- and T-component receiver functions. The Q and T receiver functions are mainly composed of the converted energy and contain information on the structure beneath a seismic station. The timing of a converted phase in receiver functions depends on the discontinuity depth and the *P*- and *S*-wave velocities
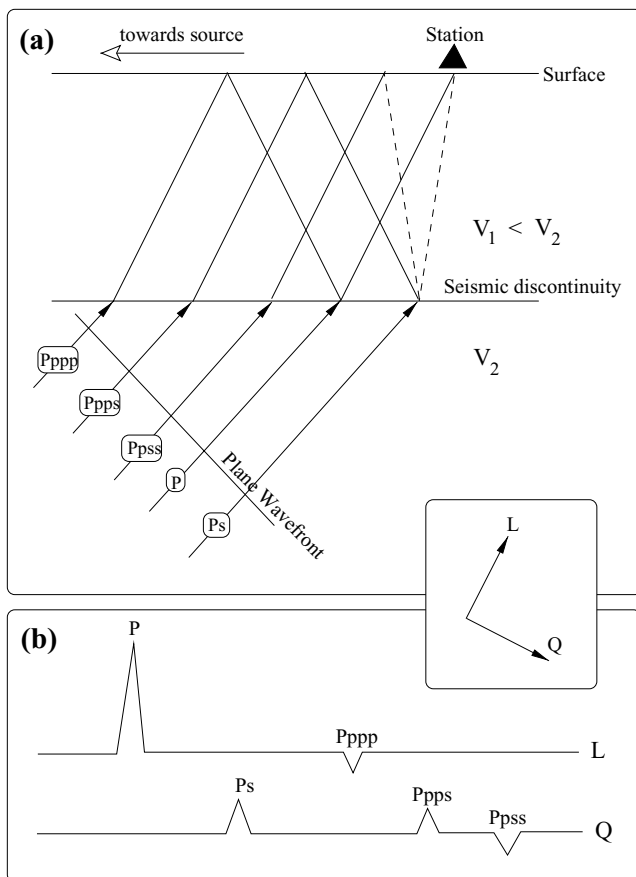
Figure 2. (a) Sketch illustrating *P–S* converted for a plane wave incident from below on a homogeneous, isotropic layer with velocity $V_1 < V_2$. The three small letters indicate the wave type of the peg legs in the multiple phases. In this notation the *P* is simply an abbreviation for *Pp*. In addition to *P–S* converted phases we show also the ray path of the *Pppp* multiple in the upper layer. (b) Schematic seismograms illustrating the various phases depicted in (a). We use a ray-based coordinate system LQT where L points in the direction of the incident *P* wave, Q is perpendicular to L and T (not shown) points out of the paper plane towards the reader. *P*-wave energy will show up mainly on the L-component, and *SV* energy mainly on the Q-component seismograms. Note that Q is positive away from the source. A velocity increase with depth will be associated for positive P with a positive amplitude for *Ps* and the first *Ppps* multiple, and a negative amplitude for the second *Ppss* multiple.

above the discontinuity. The amplitudes of converted phases depend on the *S*-wave velocity contrast across the discontinuity.

Besides the primary converted phase, a seismic discontinuity can also produce multiply reflected phases that reverberate between the discontinuity and the Earth's surface. We term the first multiples *Ppps* and *Ppss* (Fig. 2). They also appear as shear waves in the receiver functions. The multiples of the Moho often contaminate the receiver functions in the time range of 10–30 s, in which the primary converted waves from a depth range of 80–250 km arrive. However, if properly identified, these multiples provide additional information to accurately determine the depth of Moho and to estimate the crustal Poisson ratio (Yuan *et al.* 2002). A subhorizontal discontinuity will result in *P–SV* converted energy only on Q-component seismograms if the medium is isotropic. However, a dipping interface will change the ray geometry, and an anisotropic layer will cause shear wave splitting effects. In both cases converted energy is expected to be observed on the T (*SH*) components. The first-order major structures

can be extracted by analysing the Q-component receiver functions. The energy on the transverse component serves to give additional information on the crustal heterogeneity or anisotropy (Cassidy 1992; Levin & Park 1997).

The primary conversion and multiple phases from a seismic discontinuity have different moveout curves (the dependence of the wave arrival times to their ray parameters). A weak phase can be protruded out from the random noise by stacking individual receiver functions along its moveout curve (Kind & Vinnik 1988). It is also possible to make a moveout correction (the reference distance is selected to be 67°) to the individual receiver function data in a time domain and a weak phase can be identified through its amplitude coherence over the individual traces (Yuan *et al.* 1997). Since the primary converted phase and the multiples have distinctly different moveout behaviours, applying a moveout correction to a certain phase can enhance this phase and weaken the others. This is sometimes a useful method for distinguishing the primary conversions from the multiple phases.

Similar to the migration technique applied in the near-vertical reflection data, receiver functions can be migrated from the time domain to space to produce a structural image. This process requires a reference velocity model to be assumed; we chose IASP91 (Kennett & Engdahl 1991). Following Kind *et al.* (2002) we use a single-scatterer concept to migrate receiver functions. The amplitudes in the receiver functions are assumed to represent scattered energy, and are migrated into an array of point scatterers with a spacing of 2×2 km^2.

In this study we have used teleseismic records from eight broadband seismic stations located on the islands of Crete, Gavdos, Santorin, Naxos and Samos (Fig. 1b). The coordinates of the stations are given in Table 1. They are all equipped with Streckeisen STS-2 seismometers and Quanterra data loggers with the exception of KOUM, which has a Lennartz recording system. The coordinates of the stations are given in Table 1. Operation of stations at KRIS, SANT and SKD began in 1996, while the other stations were brought into operation at a later date, in 1999 (GVD) and 2000 (KOUM, APEZ, FODE and APE). Data from all the stations with the exception of KOUM are available through the GEOFON data archive under www.gfz-potsdam.de/geofon.

Broad-band seismic records of earthquakes with epicentral distances between 35° and 95° and significant *P* arrivals were selected to calculate receiver functions. Because of the uneven distribution of teleseismic earthquakes, most receiver functions are within a back-azimuth range from 0° to 90°. The number of available receiver functions at each station ranges from 13 at KOUM, ~60 at GVD and APE to more than 100 at KRIS, APEZ, FODE, SKD and SANT.

3 OBSERVATIONS

Receiver functions are shown in Figs 3–9 for the stations for which a sufficient number of observations are available to visualize some particular features in displays of single traces. Stacked receiver functions (Q-component) are shown for all stations in Fig. 10. We have marked converted phases (see also Fig. 2) from the continental Moho, and from a deeper boundary in the upper mantle that we interpret as the Moho of the descending African lithosphere. The subducting lithosphere, also referred to as the Hellenic slab, represents a large heterogeneity in the upper mantle, which is characterized by a dipping structure and a complicated morphology of the Wadati–Benioff seismic zone (Knapmeyer 1999). Slab multiples are largely disturbed by noise and can be better observed after

Table 1. Geographical coordinates of broad-band stations in Crete, Gavdos and the Aegean.

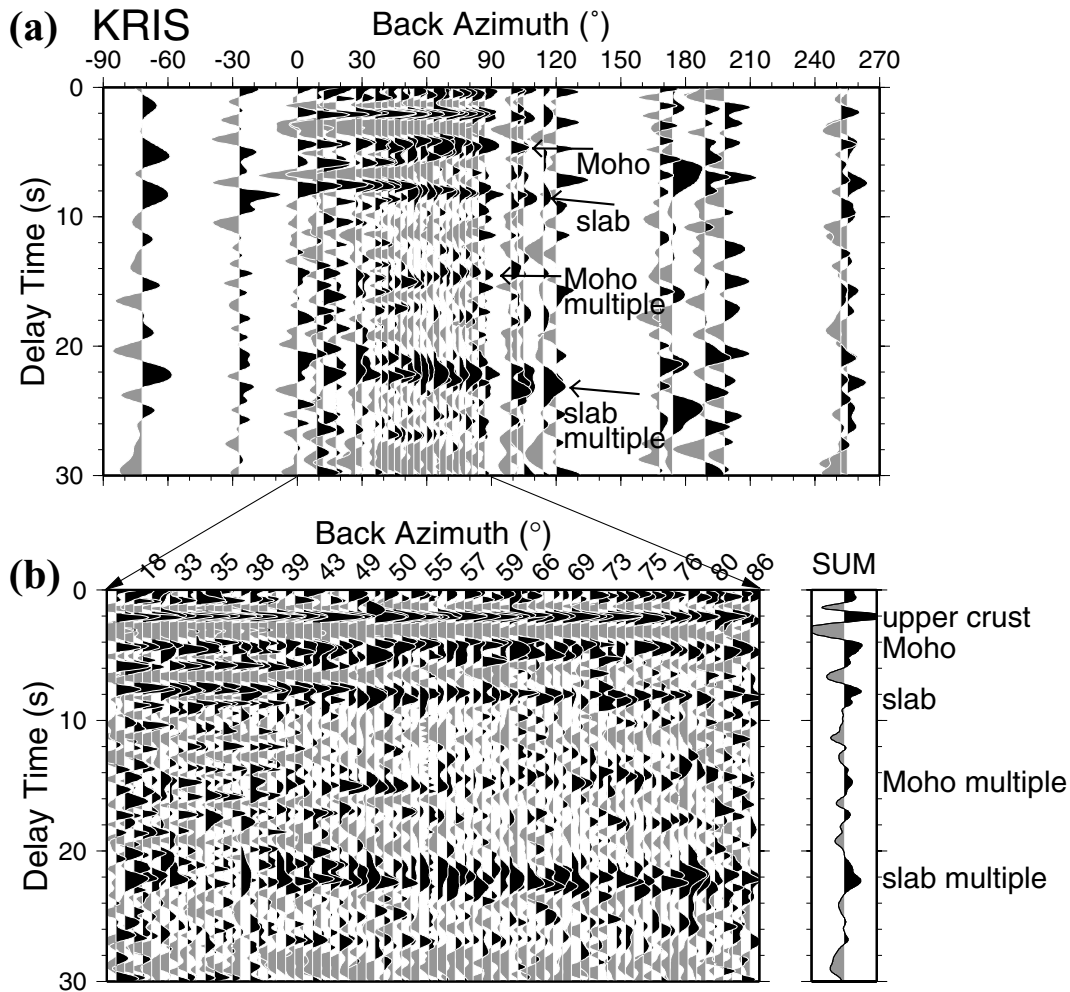| Station	Name	Latitude (°N)	Longitude (°E)	Altitude (m)	No of RFs
GVD	Gavdos	34.84	24.09	100	59
APEZ	M. Apezano	34.98	24.89	200	132
FODE	Fodele	35.38	24.96	50	142
SKD	Skordalos	35.41	23.93	700	126
KRIS	M. Kristellenia	35.18	25.50	800	118
SANT	Santorini	36.37	25.46	650	122
APE	Naxos	37.07	25.53	200	65
KOUM	Samos	37.70	26.84	200	13

Figure 3. Receiver functions for station KRIS in Crete sorted after backazimuth. In part (a) the full backazimuth range is shown, from −90° (west) through 0° (north), 180° (south) to 270° (west). A 90° section is shown with equally spaced individual receiver functions on the left and their summation trace on the right in part (b). Delay time is measured relative to the *P*-wave maximum.

a low-pass filter has been applied. The receiver functions of most of the stations exhibit clear primary Moho conversions and multiply reflected phases. For the stations that show multiple phases in the receiver functions, the Moho depth is determined by matching primary conversions and the multiples (Yuan *et al.* 2002). For other stations, the Moho depth is estimated using the IASP91 reference model. We obtained the depths of the Moho beneath our study region in the range of 25–39 km by this analysis (Table 2). The Moho boundary is deep beneath Crete and Santorini and becomes shallower to the south (Gavdos) and to the north (Naxos and Samoa). In

the following we discuss important features of the receiver functions for stations in Crete first, and then for the other stations in Gavdos and the Aegean Sea.

3.1 Receiver functions of stations on Crete

The stations KRIS and SKD are located in eastern and western Crete, respectively, while FODE and APEZ are located in northern and southern central Crete. They have produced enough data that are suitable for a detailed investigation of the structure beneath the
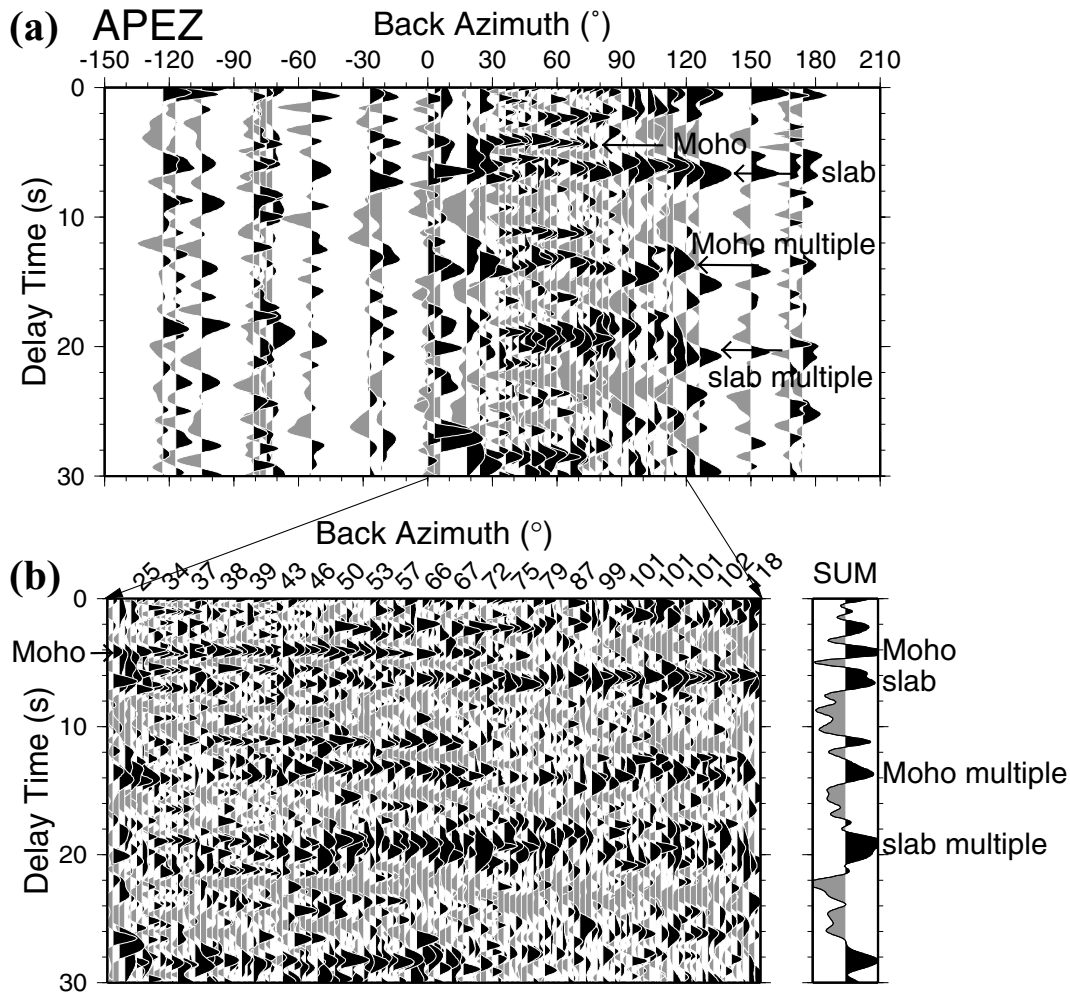
Figure 4. Same as Fig. 3 for station APEZ in southern central Crete.

stations, although the azimuthal distribution of the data is not uniform (most earthquakes occurred in the backazimuth of north to northeast). While at stations APEZ and KRIS the Moho phase can be clearly seen between arrival times of 4–5 s (Figs 3, 4 and 10), at the other two stations SKD and FODE, however, receiver functions in that time range are dominated by a significant phase with negative amplitudes (Figs 5, 6 and 10). The negative Moho conversion energy suggests a reversed velocity contrast at the crust–mantle boundary. The oceanic Moho on the descending African Plate can be observed at all stations. The depth varies between 51 and 69 km beneath the four stations.

3.1.1 Kristellenia Monastery (KRIS)

Fig. 3 shows the moveout-corrected receiver function data at station KRIS located in eastern Crete. Positive amplitude of the receiver functions are plotted in black and negative amplitudes in grey. If they are caused by primary *P–S* conversions, positive (negative) amplitudes indicate seismic discontinuities with a downward increase (decrease) of seismic velocity. In Fig. 3(a) the receiver functions are sorted by backazimuth and stacked in bins of 3°. The stacked data traces are plotted at their averaged values of backazimuth. Most of the data are from the NE direction. The primary Moho conversion, the African slab phase and the slab multiple are the clearest phases

and are labelled with their associated names. Fig. 3(b) shows the individual receiver functions from the NE backazimuth range (0°–90°) on the left and their summation trace on the right. The traces are sorted according to their backazimuth and plotted equally spaced.

Receiver functions of KRIS indicate that the crustal structure in eastern Crete is very complicated. A phase at a delay time of approximately 1 s or less may be caused by a shallow *P–S* conversion in the upper 5 km of the crust, probably the top of basement rocks. A direct *P–S* conversion from an intracrustal interface, labelled as 'upper crust', stands out at approximately 2 s delay time corresponding to a conversion depth of approximately 19 km. This boundary may represent the transition from upper to lower crust. The phase at approximately 3.5 s delay time, which has consistently negative amplitudes may represent a low-velocity layer in the lower crust. The Moho and its *Ppps* multiple are also marked in Fig. 3(b). Using the delay times of both primary Moho conversion and its multiple, the Moho beneath KRIS is estimated at 34 km depth (Table 2). The average slab depth is 69 km.

The Moho conversion shown in Fig. 3 seems to be composed by two sharp phases in NNE direction of the station (backazimuth 0°–45°), while this double phase is not seen in other directions. This 'double phase' may represent a complex interference of the multiple from the upper-to-lower crust boundary or structure in the sub-Moho mantle. However, the observation that a similar
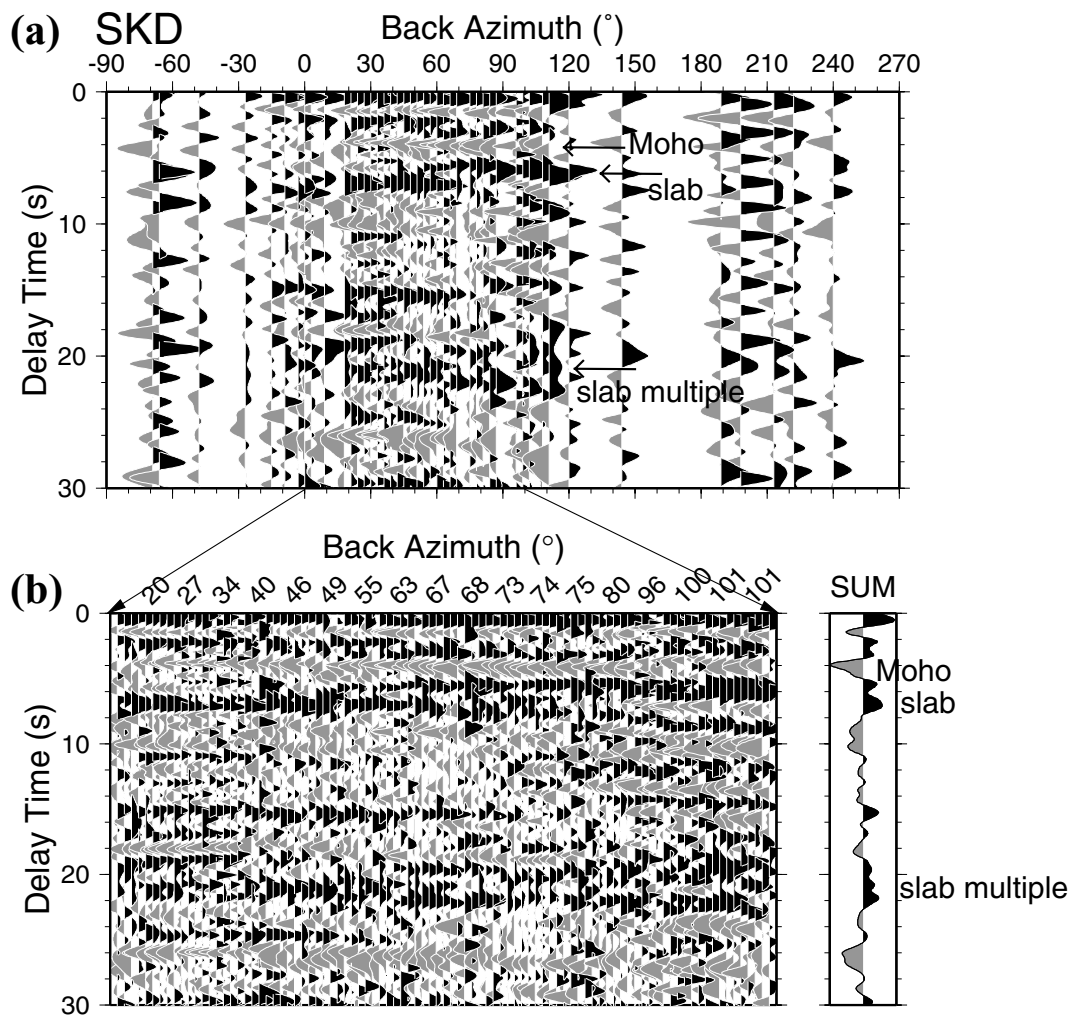
Figure 5. Same as Fig. 3 for station SKD in western Crete.

bifurcation also appears in the slab *P–S* conversion is evidence against such interpretations. These lateral variations rather imply a quite complicated structure at shallow depth which is difficult to image in more detail with data from just one station.

3.1.2 Apezano Monastery (APEZ)

The station APEZ is located in southern central Crete, at the southern edge of the Messara plane. The Moho and the top of the descending Hellenic slab could be reliably imaged on the basis of primary conversions and associated multiples. In Fig. 4(a), the data are stacked within 5° bins in backazimuth and plotted at their average backazimuthal values. Individual data traces for events from the NE direction are plotted equally spaced in order of their backazimuths (Fig. 4b). The primary and the multiple phases from the Hellenic slab are observed independent of backazimuthal direction. The Moho conversion, however, is clearly observed only north and northeast of the station. There may be several reasons for this. Multiples from innercrustal discontinuities that vary laterally in structure and depth extent may mask Moho conversions. The Moho may possess significant topography or variations in sharpness. The Moho, where it can be observed, and the slab beneath this station are at 31 and 51 km depth, respectively (Table 2).

3.1.3 Skordalos (SKD)

The station SKD is located in western Crete, at an altitude of approximately 800 m. A good database exists for this station. The SKD receiver functions (Fig. 5) are characterized by the absence of direct *P–S* conversions from the Moho. At the time range of the expected Moho conversion (∼4 s) a strong negative phase appears. The phase is much more prominent in the data of north-to-east backazimuth range (Fig. 5b). The same phenomenon is also reported by another study of teleseismic receiver functions from a station network located in this region Knapmeyer & Harjes (2000). We interpret the phase with negative amplitudes as a reversed velocity contrast at the crust–mantle boundary. The underlying mantle has lower shear wave velocity than the overlying lower crust. We attribute this phenomenon to hydration and serpentinization of the forarc mantle wedge. A significant quantity of serpentinite in the underlying mantle wedge can dramatically reduce the elastic wave velocity in the mantle, causing a reversed Moho velocity contrast. Similar observations have been made in the Cascadean subduction zone by Bostock *et al.* (2002). We will discuss this issue later in this paper. The Moho multiples are difficult to recognize from the receiver function data. Assuming the IASP91 crustal velocities, we estimated the Moho depth to be 32 km. The converted wave at the Moho of the downgoing slab arrives at a time of ∼7 s.
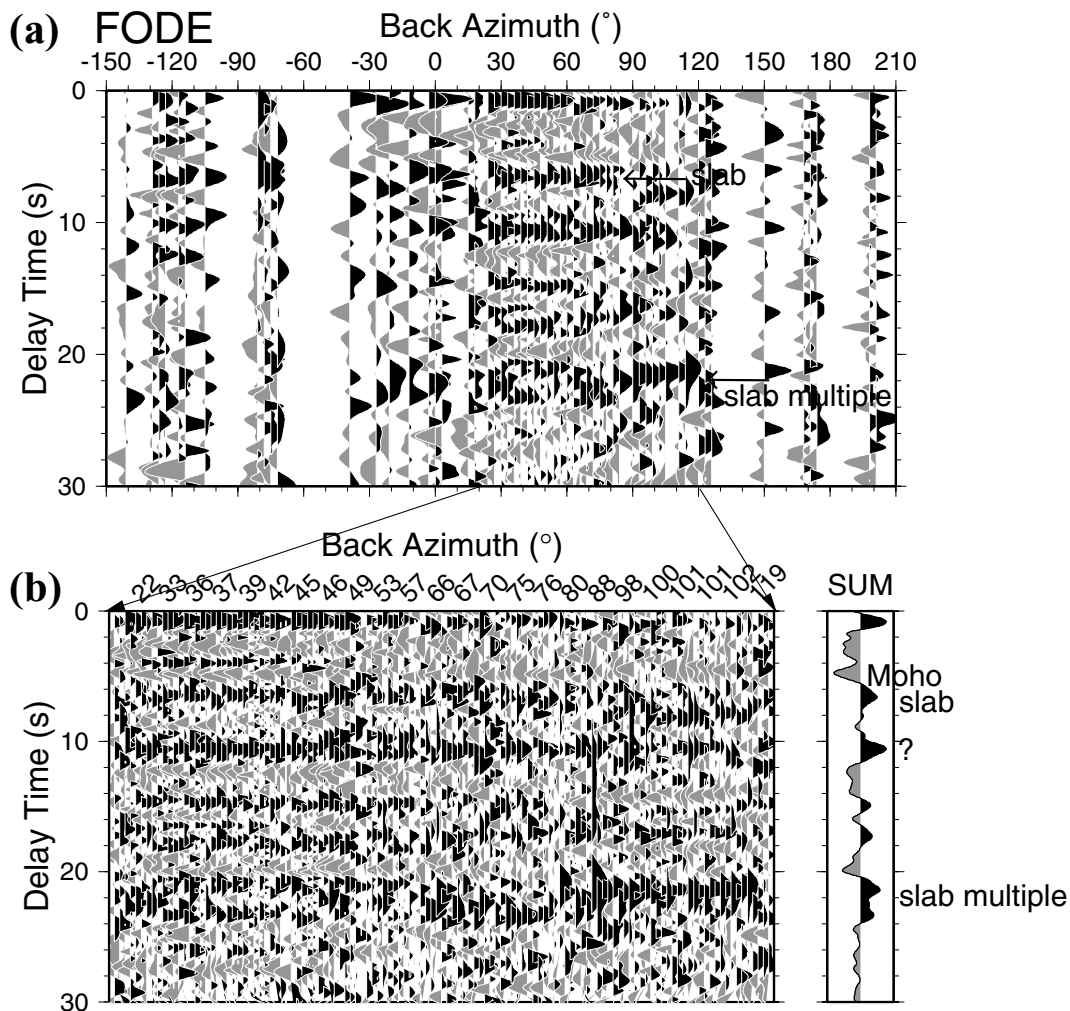
Figure 6. Same as Fig. 3 for station FODE in northern central Crete.

We obtained an average depth of the slab of 63 km beneath this station.

3.1.4 Fodele (FODE)

At station FODE clear phases are the primary conversion from the slab at 6.7 s and its multiples at ∼22 s (Fig. 6). Another coherent phase is observed at 11 s delay time. The nature of this phase is unclear. If it is a real converted phase, it should indicate a discontinuity at a depth of 90–100 km in the upper mantle. Similarly to station SKD, positive Moho conversions in the time window of 4–5 s are not indicated by the data. Instead, a phase with negative amplitudes can be identified at a time of 4.8 s. Although the contamination of multiple phases from shallower layers cannot be exclusively ruled out, this negative phase is unlikely to be caused by multiples alone, because there appear to be no possible layers at the shallower depth generating multiple phases at the corresponding time. Our interpretation is similar as that of station SKD. The negative phase at a time of 4.8 s is *P*-to-*S* conversion at the Moho of negative velocity contrast. The amplitudes of the negative Moho phase are, however, smaller compared with those of station SKD. This suggests a smaller crust–mantle velocity contrast beneath station APEZ. The depth of the Moho is estimated to be 39 km using the ISAP91 model.

3.2 Receiver functions of stations on other islands

3.2.1 Santorini (SANT)

Significant crustal heterogeneity is inferred from the receiver function data of station SANT on Santorini. Receiver functions of SANT exhibit strong coherent off-azimuth energy on the transverse component. Figs 7(a) and (b) show stacked T- and Q-component receiver function data binned in 3° intervals of backazimuth and plotted at their average backazimuth values. In Fig. 7(c) the individual Q-component receiver functions are plotted equally spaced in order of backazimuth from 0° to 120°. In Q-component data (Figs 7b and c) some primary conversions and multiples are identified for different interfaces and are marked with their associated names. The average depth of Moho and the inferred slab here is 32 and 99 km, respectively (Table 2). Another converting boundary seems to be present at shallower depth, at approximately 25 km (corresponding to 2.5 s delay time), but this is seen only in a backazimuthal range from north to east (Fig. 7c).

A previous receiver function study reported 24 km crustal thickness beneath station SANT Priestley *et al.* (2000). We think the reason for the discrepancy is the complicated behaviour of the Moho conversion phase and incomplete azimuthal data coverage in their data collection. With much more data added we see more details of the Moho phase. In the following we will show that the
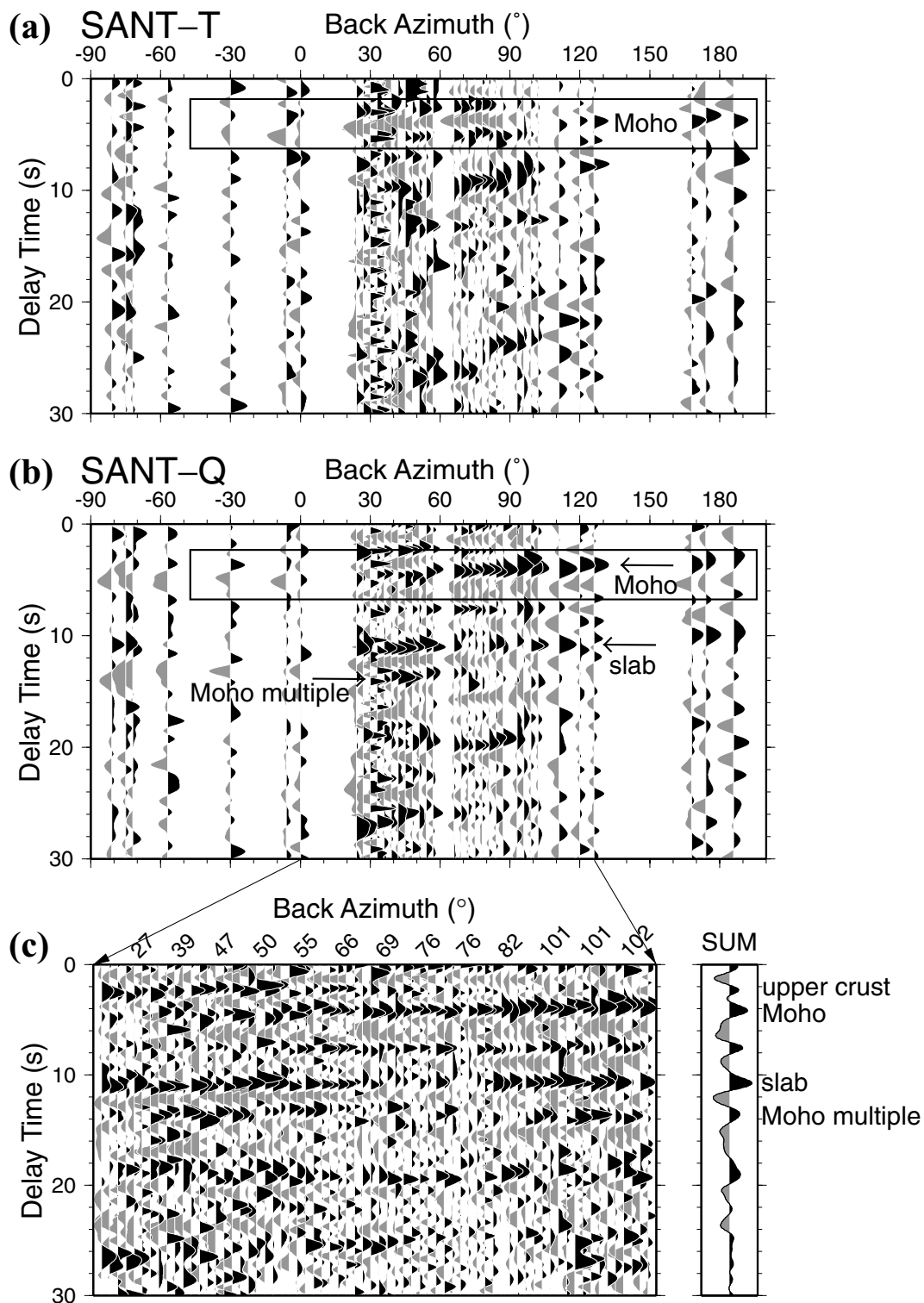
Figure 7. Receiver functions for station SANT in Santorini island sorted after backazimuth. Similar arrangement for parts (b) and (c) as in Fig. 3. In (a) transverse component receiver functions are shown. Note the coherent energy at 4 s delay time with polarity reversal between backazimuth of 90° and 110°.

peculiar Moho behaviour can be conveniently modelled with crustal anisotropy.

The situation is particularly complex for the Moho phase seen at 4 s delay time on the Q-component that seems to arrive earlier from the east and south than from the north (Fig. 7b). The amplitudes

on the Q-component are largest in backazimuths between 90° and 120°. This phase has a coherent energy at ∼4 s on the T-component (Fig. 7a). Although the azimuthal distribution of receiver functions is poor, a polarity reversal on the T-component can still be identified between 90° and 120°. From north to east (0°–90°) the T-component
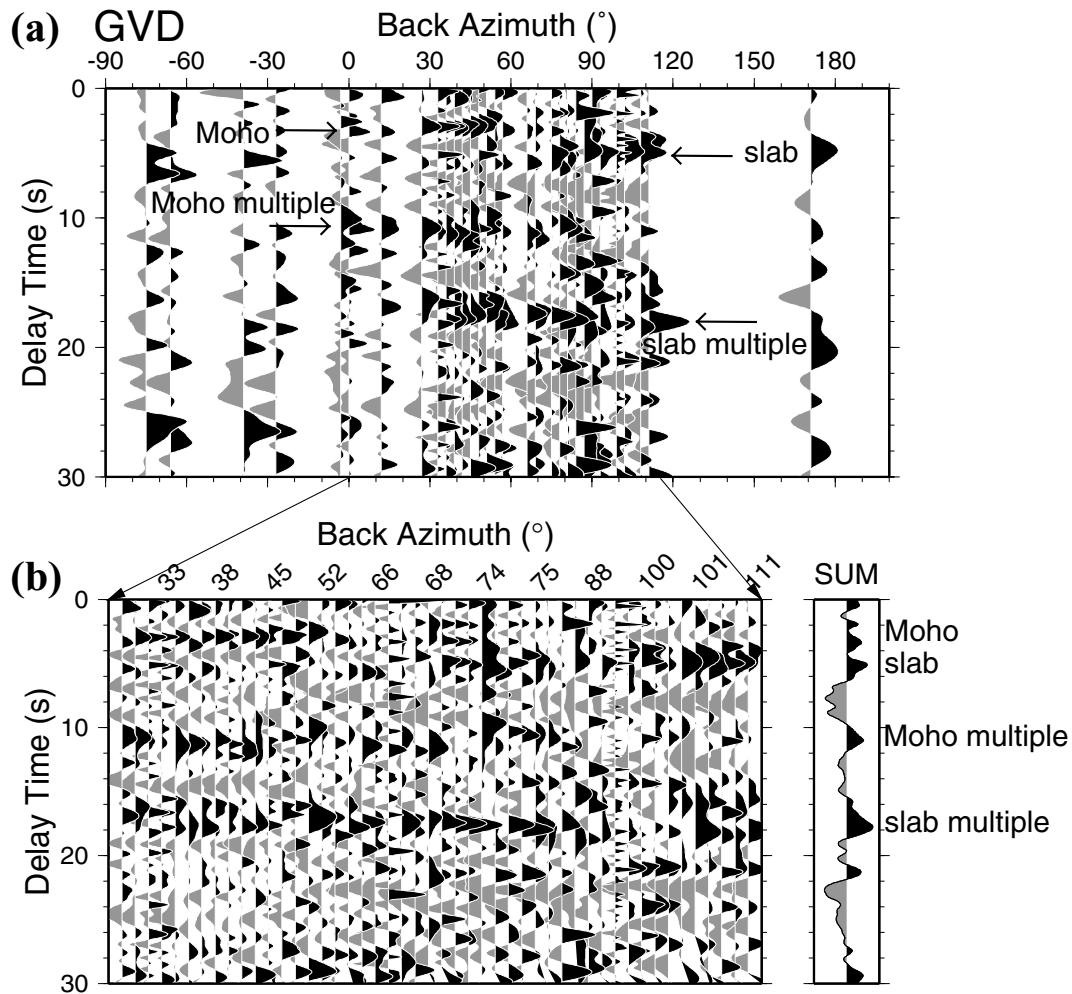
Figure 8. Same as Fig. 3 for station GVD in Gavdos island.

has negative amplitudes at ~4 s, whereas from east to south (110°–180°) this phase becomes positive. There are two usual ways to explain the coherent energy on the transverse component. The first explanation assumes that the Moho is a dipping interface. In the Q-component the converted wave at the Moho has stronger amplitudes in the downdip direction and is weaker in the updip direction. In the T-component, no off-azimuth energy will be generated in the downdip or updip direction (within the incidence plane), whereas, in the two sides of the incidence plane, the T-component has different polarities (see Cassidy 1992, for more details). According to this explanation the Moho beneath SANT seems to dip to the east. Alternatively, the other explanation uses crustal anisotropy (Levin & Park 1997). An anisotropic crust in a flat layer can produce similar phenomena to a dipping interface: the amplitude variation in the Q-component and the polarity reversal in the T-component. However, there are two facts in the data to prevent us from choosing the dipping Moho as a final model. (1) An unrealistic large dip angle of ~40° is needed to explain the big arrival time variation in the Moho conversions on the Q-component between backazimuths of 30° and 120° (Fig. 7b). (2) The Moho conversion arrives earlier by ~0.5 s on the T-component (Fig. 7a) than on the Q-component (Fig. 7b), indicating shear wave splitting in the crust. Therefore, we prefer a model of crustal anisotropy. We calculated synthetic receiver functions for several models of horizontal anisotropic crustal layer using

a reflectivity procedure (Levin & Park 1997). In Fig. 11 we show a model that can explain the phenomena we observed in the data. The model includes a single crustal layer of hexagonally symmetric isotropy with a thickness of 32 km. The symmetric axis is tilted 45° from vertical and in azimuth of 105° from north. We use an oblique symmetric axis that is inclined from vertical in order to simulate the polarity pattern of the Moho phase on the T-component, which has a variation period of 360° azimuth (Fig. 7a). Levin & Park (1997) has shown that a horizontal symmetric axis of isotropy will cause the phase polarity on the T-component to change with an azimuthal period of 180°, whereas an oblique axis gives rise to polarity changes with 360° period. Although the crustal anisotropy usually has a slow polarization axis (Levin & Park 1997), a fast polarization axis is need for station SANT to fit the time and amplitude variations in the T-and Q-component receiver function data. We tentatively give 8 per cent to the strength of anisotropy, equally applied for *P* and *S* waves. The model parameters are listed in Table 3. Because the anisotropic inversion is non-unique (too many parameters to change), there are of course other anisotropic models that fit the data well, e.g. a finite layer of anisotropy near the Moho. We did not intend to model every detail in the data and discuss crustal anisotropy in details in this paper. Our purpose is to use this simple model to simulate the Moho conversion phase at ~4 s on the Q- and T-components and to verify our crustal thickness. We plotted the synthetic receiver
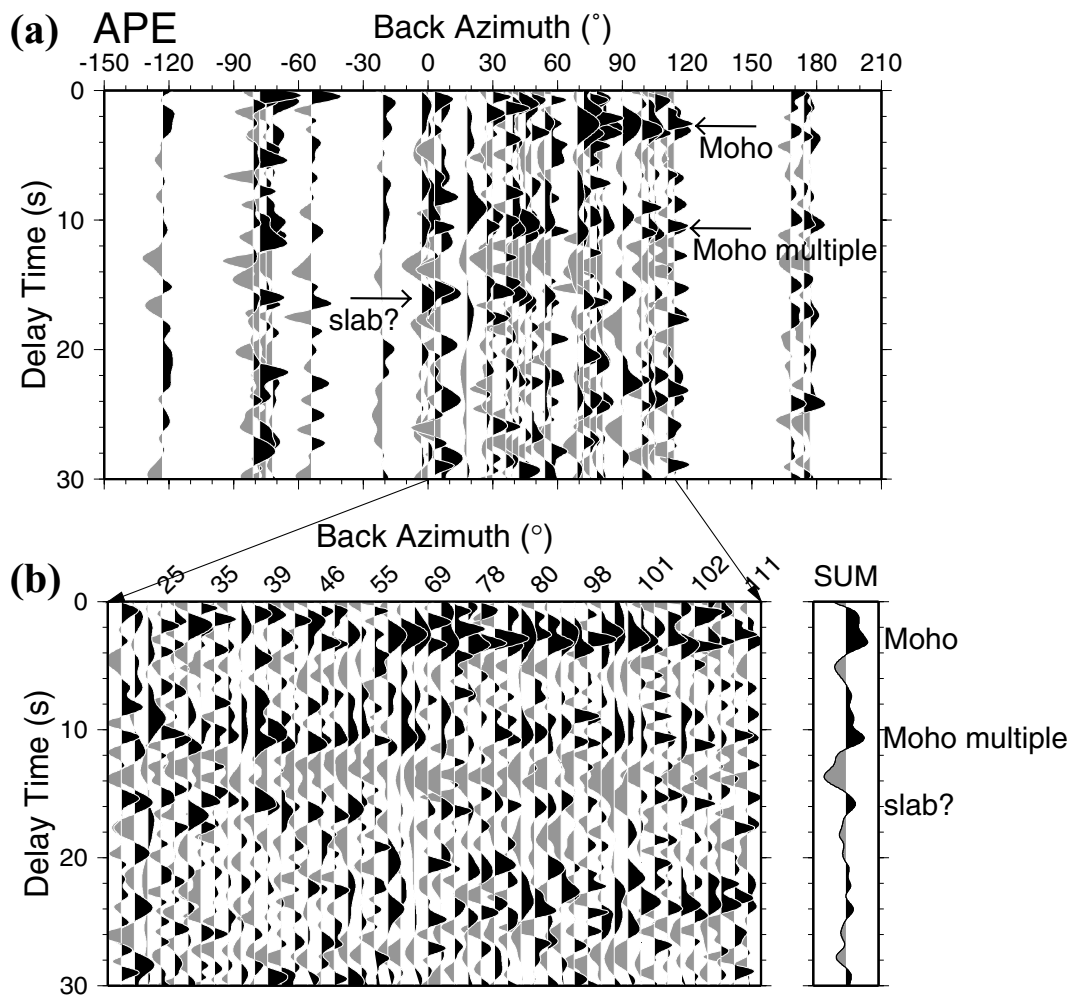
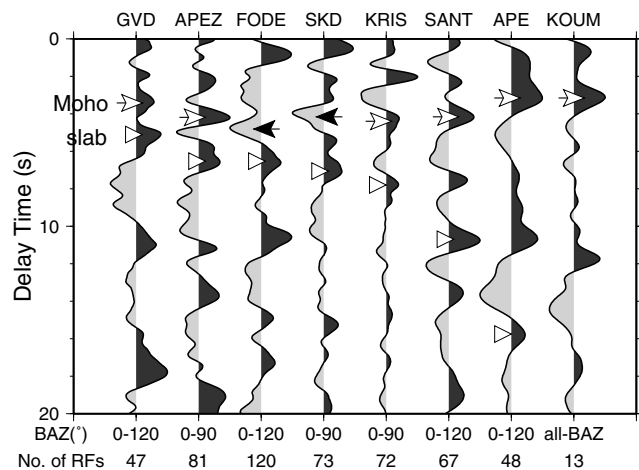**Figure 9.** Same as Fig. 3 for station APE in Naxos island.

Figure 10. Stacked receiver functions for station in Gavdos, Crete and in the Aegean. The backazimuthal ranges and the number of individual traces used is shown in the bottom of the figure.

function within a time window of 10 s. In Fig. 11 we can see that the synthetics simulate the data very well in all the following aspects: the amplitude and time variations in the Q-component; the polarity reversal in the T-component; the time difference between the Q- and T-components.

Table 2. Measured delay times of Moho and slab conversions and the inferred depths.

Station	Moho			Slab	
	T_{Ps} (s)	T_{Ppps} (s)	H (km)	T_{Ps} (s)	H (km)
GVD	3.3	11.0	26	5.3	44
APEZy	4.3	13.7	31	6.1	51
FODE	4.8	—	39	6.7	57
SKD	4.0	—	32	7.3	63
KRIS	4.4	14.7	34	8.0	69
SANT	4.3	13.6	32	11.1	99
APE	3.1	10.6	25	16.2 (?)	147 (?)
KOUM	3.3	11.7	28	—	—

3.2.2 Gavdos (GVD), Naxos (APE) and Samos (KOUM)

Besides the stations on Crete and Santorini, we also used data from a station on the island of Gavdos located south of Crete (GVD on Gavdos) and in the Aegean Sea to the north of Crete: Naxos (APE) and the MIDSEA station on Samos (KOUM). The noise level of stations GVD and APE is relatively high. This can also be seen in the receiver function data (Figs 8 and 9). The available receiver function data at KOUM are relatively few so that we discuss the main results with the summation trace for this station (Table 2 and Fig. 10).
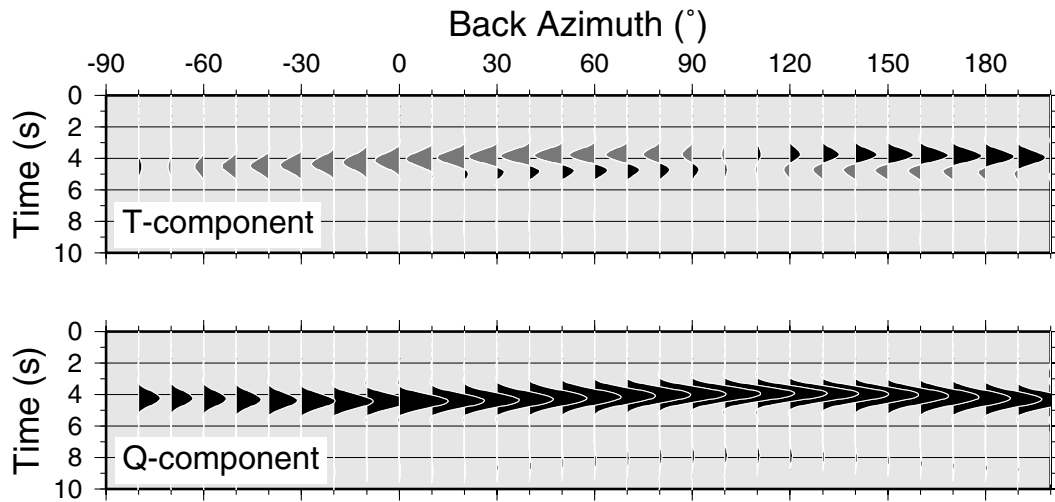
Figure 11. Synthetic receiver functions calculated for an anisotropic crustal model. The fast axis of the hexagonal isotropy model is tilted 45° from the vertical and is in backazimuth of 105° from the north.

A primary Moho *P–S* conversion and its multiple can be recognized at all these stations. Estimated Moho depths are 26 km beneath GVD, 25 km beneath APE and 28 km beneath KOUM. The primary *P–S* conversion from the Hellenic slab arrives at GVD probably right after the Moho conversion at approximately 5 s, which corresponds to a conversion depth of approximately 44 km (Fig. 8). The associated *Ppps* multiple can be seen at ∼17 s delay time.

In the individual receiver functions of APE (Fig. 9), a phase with positive amplitude appears at approximately 16 s delay time. If this is a primary conversion, the inferred depth would be approximately 147 km, which corresponds to the depth of the seismic zone beneath Naxos. The Moho conversion at ∼3 s is diffuse. The phase seen at 10–11 s delay time represents a *Ppps* multiple associated with the Moho and the subsequent negative phase at 13–14 s delay time is the corresponding *Ppss* multiple.

In the summation trace for KOUM (Fig. 10) the primary Moho phase, the Moho *Ppps* and *Ppss* multiples are clearly seen at times of 3.3, 11.7 and 14.5 s, respectively. A phase with positive amplitude shows up at ∼18 s, implying a depth of 170 km for a primary *P–S* conversion. It is not possible to answer with certainty the question of whether this indeed represents a *P–S* conversion from the deeper parts of the Hellenic slab. This is related to the few data of KOUM and the large spatial spacing of stations. Tomographic images of the Hellenic subduction zone (Spakman *et al.* 1988) show high-velocity anomalies extending to 600 km depth, but converted phases from descending slabs of oceanic lithosphere are usually not observed from deeper than approximately 200 km (Abers 2000; Bock *et al.* 2000; Li *et al.* 2000; Yuan *et al.* 2000).

4 DISCUSSION OF RESULTS

Results are summarized by the stacked receiver function data shown in Fig. 10. Except for KOUM, stacking proceeded to the receiver functions within the backazimuths between north and east. Stack-

ing was carried out after correcting the individual broad-band data for moveout, choosing a reference slowness of 6.4 s deg^{-1} corresponding to an epicentral distance of 67°. The summation traces reveal an average structure beneath each station. The depth values of the Moho and of the slab listed in Table 2 were calculated from the summation traces. The stations are sorted by increasing time of the interpreted slab phase, which is indicated in Fig. 10 by the open triangles. The primary Moho phases are also marked by white and black arrows where they could be identified.

On Crete, clear normal Moho phases are observed only at KRIS and APEZ. The inferred Moho depths beneath these stations (Table 2) are consistent with a continental-type Moho, and they generally agree with results from controlled seismic experiments and gravity field modelling (Makris 1976; Bohnhoff *et al.* 2001). No clear direct Moho conversions with positive amplitudes are seen at the stations SKD and FODE. Instead, significant converted phases with negative amplitudes appears at 4.0 s at station SKD and at 4.8 s at station FODE. The same phenomenon is also reported by another study of teleseismic receiver functions from a station network located in western Crete (Knapmeyer & Harjes 2000). Knapmeyer & Harjes (2000) modelled the receiver functions observed in western Crete with a model of a 15–20 km thick crust underlain by a low-velocity zone. They argue that the crust proper of the overlying Aegean Plate, including Crete, is only approximately 20 km thick, and is underlain by a subducted accretionary wedge of low-velocity material. Earlier models by Makris (1976) that are based on a combined interpretation of seismic and potential field data postulate a 30–33 km thick crust beneath western Crete, while Bohnhoff *et al.* (2001) inferred a crust of variable thickness ranging from 24 to 26 km beneath eastern Crete to 32–33 km beneath northern central Crete.

We interpret this negative conversion energy as a reversed shear velocity contrast on the crust–mantle boundary. The underlying mantle has lower shear wave velocity than the overlying lower crust.

Table 3. The anisotropic velocity model for the synthetic receiver functions in Fig. 11.

Depth (km)	V_P (km s^{-1})	V_S (km s^{-1})	ρ (g cm^{-3})	Strength of anisotropy	Azimuth of fast polarization axis	Tilt of fast polarization axis
32	6.2	3.4	2.7	8 per cent	105°	45°
∞	8.1	4.5	3.3	0	—	—

Considering the hydration and dehydration processes associated with the subduction of the oceanic crust, we attribute the anomalous behaviour of the Moho property to hydration and serpentinization of the forearc mantle wedge. The significant amount of serpentinite in the underlying mantle wedge can dramatically reduce the elastic wave velocity in the mantle, causing a reversed Moho velocity contrast (Ulmer & Trommsdorff 1995; Giese *et al.* 1999; Bostock *et al.* 2002; Hyndman & Peacock 2003).

When oceanic plates subduct, much of water will be released from the oceanic crust, hydrate the upper-plate continental mantle and cause stabilization of hydrous mantle minerals such as serpentinite. The serpentinites contain up to 13 per cent water by weight and are stable in the upper mantle at temperature below 720 °C (Ulmer & Trommsdorff 1995; Hyndman & Peacock 2003). In forearc mantle the temperature is usually low, less than 600 °C. The temperature increases beneath the arc and the backarc to more than 800 °C. Therefore, serpentinites can only exist in the forearc region and become unstable in arc and backarc regions. The degree of serpentinization in the forearc depends on the water content and the temperature condition. Serpentinite has seismic wave velocities much slower than that of the normal mantle. The shear wave velocity of fully serpentinized peridotites can be reduced by ~2 km s^{-1}. Assuming a lower-crustal shear velocity of 3.6 km s^{-1} and a degree of serpentinization of 50 per cent, the shear velocity of the uppermost mantle can be lower by 10 per cent than that of the lower crust (Bostock *et al.* 2002; Hyndman & Peacock 2003).

Crete island is located in the forearc region in the subduction zone of the African and Eurasia plates. The forearc mantle beneath Crete island is hydrated and contains a significant quantity of serpentinite. Consequently, the elastic wave velocity of the upper-plate mantle beneath Crete may be relatively low. The serpentinization is, however, heterogeneous and not taking place uniformly beneath Crete island. Beneath western Crete the highest degree of serpentinization would be achieved. This could be indicated by the abnormally large negative Moho conversion amplitudes in the receiver functions of station SKD. In northern central Crete, receiver functions of station FODE also display a negative Moho conversion phase. Because of the existence of a significant quantity of serpentinite beneath both stations, the shear velocity in the uppermost mantle is lower than that of the lower crust, causing a reversed Moho velocity contrast. At other two stations KRIS and APEZ, located in the eastern and southern central Crete, respectively, we observed positive conversions of the Moho, implying that the amount of serpentinite is not large enough to effectively reduce the mantle shear velocity to be less than that of the lower crust.

We conclude that the crustal thickness beneath Crete island is between 31 and 39 km depth. Beneath western and northern central Crete, the mantle shear wave velocity is lower than that of the lower crust, causing an unusual reversal of the Moho velocity contrast.

Beneath Gavdos, however, the Moho is only at 26 km depth, a value that is also observed in the Aegean Sea. A necessary condition for uplift to occur in Crete under extensional forces is that the descending African lithosphere is mechanically decoupled from the overlying plate (e.g. Angelier *et al.* 1982). If the two plates were mechanically coupled, Crete would be subject to subsidence. If the crust were indeed as thick as 35 km, the decoupling zone between the descending Hellenic slab and the overlying Cretan crustal block would be only approximately 5–15 km thick.

At the Aegean stations SANT, APE and KOUM the Moho is seen between 25 and 32 km depth. We have no data for the Sea of Crete, between Crete and Santorini, where Bohnhoff *et al.* (2001) reported a shallow Moho at 15 km depth. This would imply very strong thinning

of the crust occurring in this area in comparison to the Aegean crust north of the volcanic arc. The extent of thinning would be much stronger than that inferred by (Angelier *et al.* 1982), who based their calculations on a simple stretching model and a Moho depth of approximately 25 km. It has been noted Avigad *et al.* (2001) that extensional tectonics affecting the central Aegean during the last 15–20 Myr have not produced a significant net crustal thinning. Our results of the Moho depths for SANT, APE and KOUM suggest that low to moderate crustal thinning has occurred over the past 15–20 Myr if we assume that the Aegean crust was continental prior to the inception of the extensional regime. Adopting stretching factors of 1.2–1.4 for the central Aegean (Angelier *et al.* 1982) and an average crustal thickness of 25 km, crustal thickness at the time of the onset of the extensional regime would have amounted to between 30 and 35 km.

The crust beneath most of the stations is highly anisotropic. Coherent energy on the transverse component can be observed at many stations. At station SANT on Santorini island significant energy on the transverse component correlates well with the primary Moho conversion on the radial component (Figs 7a and b). Synthetic receiver functions (Fig. 11) calculated with an anisotropic crustal layer fit well the Moho phase on both T and Q components. The crustal anisotropy is usually attributed to fine-layering, cracks or melt lenses, which cause a slow axis of symmetry. The mantle anisotropy is more likely to have a fast polarization axis, caused by lattice preferred orientation of olivine crystals. However, a fast polarization axis is need for station SANT to fit the time and amplitude variations in the T- and Q-component receiver function data. The inferred fast polarization-axis points approximately to the east (backazimuth of 105°) with an inclination of 45° from the vertical. Therefore, the anisotropy in the crust beneath SANT could not be caused by stacks of fine layers or cracks in the upper crust, rather it may possibly be associated with the fossil or current strain accumulation and deformation or trench-parallel flow in the lower crust, resulting from the subduction and collision processes. The crustal anisotropy is, however, obviously different from the mantle anisotropy derived by *SKS* splitting (Hatzfeld *et al.* 2001). The shear wave splitting in the mantle is weak and is determined to have the fast polarization direction in backazimuth of 30°. The discrepancy could imply that the crust beneath Santorini is possibly decoupled from the upper mantle with the subduction and collision processes.

The individual broad-band receiver functions were migrated into the space-domain and projected on to a depth section of SSW to NNE direction passing through GVD and KOUM (Fig. 12). This direction is approximately parallel to the dip direction of the Wadati–Benioff zone. In Fig. 12 we show two sections of different depth ranges with different resolutions. The depth range in (a) is 0–150 km, intended to show the Hellenic slab phase beneath Crete and Santorini. Seismicity is projected on to the section (black dots), after Engdahl *et al.* (1998). Positive amplitudes of the receiver function are shown in red and negative in blue. The slab phase in this image is consistent with the seismicity and it is clearly observed under Gavdos, Crete and Santorini over the depth range from 40 to approximately 100 km. This phase may continue to nearly 150 km depth under Naxos and more to the north (see also Fig. 10). However, the large gap between the stations and the weakening of the slab phase prevents us from following a possible slab phase to greater depth. Where it is observed, the slab phase clearly has a positive amplitude, implying a sharp velocity increase with depth. This is interpreted as the oceanic Moho of the descending African lithosphere. The velocity contrast is large if the phase transition to eclogite in the cold descending oceanic crust is delayed (Peacock 1993). Our observations suggest
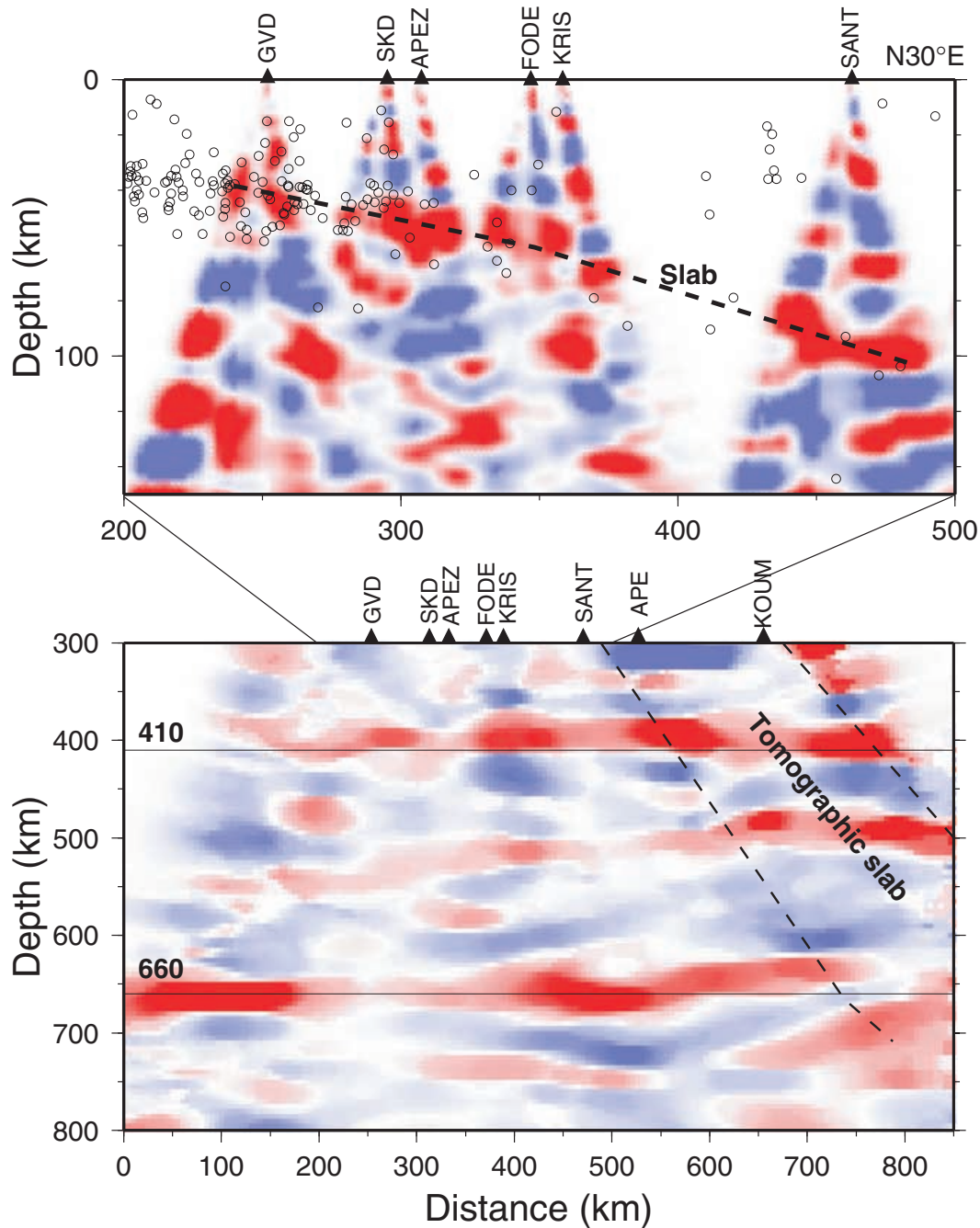
Figure 12. Migrated receiver function transect (N30°E) from Gavdos through Crete extending into the Aegean (KOUM). The IASP91 model is used as reference velocity model. (a) Section of 0–150 km depth range. The term 'slab' denotes *P–S* conversions from the Moho of the subducting African lithosphere. This can be followed from Gavdos to Crete at depths from 40 to nearly 70 km. Beneath SANT the slab is at ∼100 km depth. Further north in the Aegean the continuation of the 'slab' phase is less clear. Small circles indicate earthquake hypocentres projected on to the transect (Engdahl *et al.* 1998). (b) Section of depth range 300–800 km, showing the upper mantle transition zone. Dashed lines indicate the downgoing slab by seismic tomography (Spakman *et al.* 1988). The two thin lines mark the discontinuities at 410 and 660 km. The observed 660 is at its normal depth while the 410 is at ∼400 km depth. The transition zone here is ∼10 km thicker than that of the IASP91 model. Weak indication of the 520 km discontinuity exists beneath the northern part of the section.

that the transition to eclogite is delayed to at least 100 km depth in the subducting cold oceanic crust. In Fig. 12(b) the migrated receiver functions are shown in a depth range of 300–800 km. A spatial smoothing window of 40 km is applied over the section to enhance the phase correlation of the upper-mantle discontinuities. The two discontinuities at depths of 410 and 660 km are seen clearly and continuously. While the 660 km discontinuity is at its normal

depth (660 km), the 410 is ∼10 km shallower at ∼ 400 km depth. The transition zone, defined between the two discontinuities, is approximately 10 km thicker than predicted by the IASP91 model. The thickness of the mantle transition zone normally related to the temperature variation in the surrounding mantle. A 10 km thicker transition zone indicates a temperature reduction of ∼80° (see e.g. Helffrich 2000). Our stations are located south of the area where
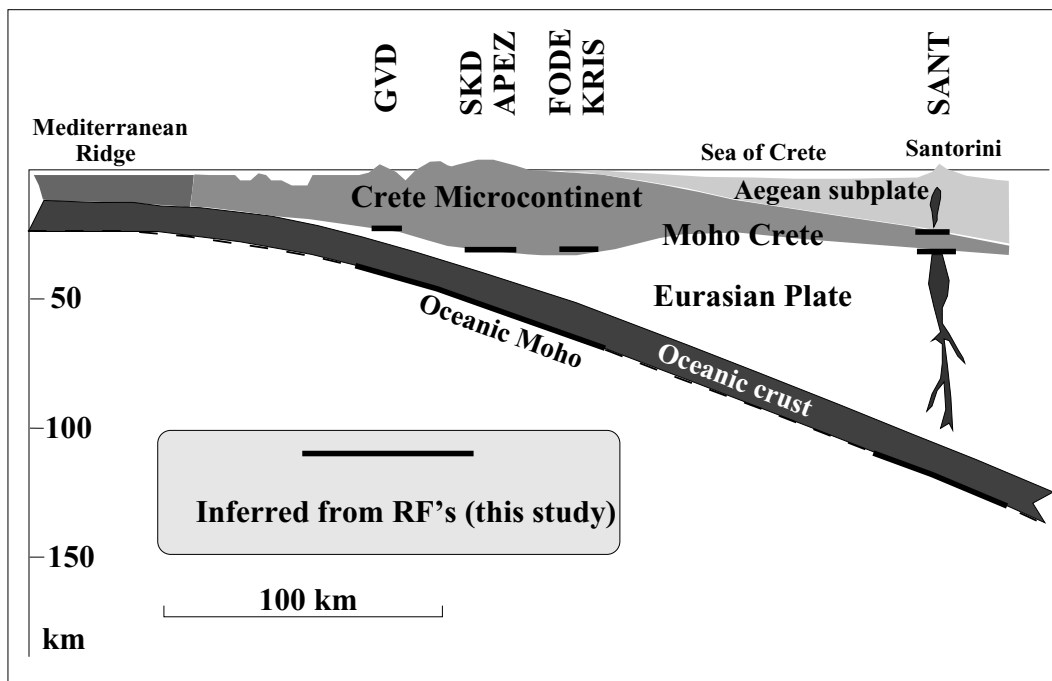
Figure 13. Transect normal to the plate boundary of the Hellenic arc, after Papanikolaou *et al.* (1999). Structural elements inferred from our receiver function analysis are shown. The Moho beneath Crete is imaged by positive primary *P–S* conversions in central and northern Crete and in western and southern Crete by negative conversions at a serpentinized upper mantle.

the downgoing slab encounters the mantle transition zone. Therefore, the data sample the African mantle. The conversion from the 410 km discontinuity arrives relatively early to the IASP91 model, indicating a fast upper mantle in the southern Aegean. In the mantle beneath oceans, however, the 410 km discontinuity has normally later arrivals and the transition zone is relatively thin (Li *et al.* 2003). The observed temperature variation in the transition zone seems not be to related to the subduction processes. It rather suggests that the whole underlying mantle is relatively cold at a large lateral scale.

In Fig. 13 we summarize our results within a conceptual framework for the present-day tectonic situation of the Hellenic arc. We discuss our results in relation to a hypothetical transect suggested by Papanikolaou *et al.* (1999) and based on geological, geophysical and geodetic observations describing the evolution of the Hellenic subduction zone (e.g. Le Pichon & Angelier 1979; Makropoulos & Burton 1984; Jackson 1994; Le Pichon *et al.* 1995). In this conceptual model, Crete forms a horst-like structure which is part of the Aegean subplate. It extends to the SSW to the backstop with the Mediterranean ridge which is considered to form the present-day accretionary wedge and where the deformation front (Fig. 1a) is close to the African coast.

Seismic discontinuities that we observe in the receiver functions are marked in the image of Fig. 13. The Moho under Gavdos, Crete and the Aegean stations are well supported by the observations, and so are the phases from the oceanic Moho of the Hellenic slab. The boundary seen at Santorini at approximately 25 km depth, inferred from a *P–S* conversion at 2.5 s delay time, may represent the shear-coupled detachment zone between the bottom of the Aegean subplate overlying the top of the microcontinent of Crete. The bottom boundary (the Moho) of the microcontinent causes the *P–S* conversion seen at Santorini at 4 s delay time. This boundary is separated from the detachment zone and lies at a depth of 30 km or a bit deeper. The interpretation is hampered, of course, by the fact that we have no data that allow us to trace these boundaries

through the Sea of Crete. Bohnhoff *et al.* (2001) derived a value of 15 km for the crustal thickness in the Sea of Crete based on reflection seismic data. However, maximum offsets were only 60 km; so one cannot rule out the possibility that deeper discontinuities could not be imaged by wide-angle reflections. The question of whether the boundary at 25 km depth beneath Santorini can be traced further south into the Sea of Crete cannot be answered on the basis of the receiver function data from land-based stations. In a current study still under progress, we have found evidence for a boundary at that depth from *S–P* converted waves that are recorded from deep events (depth > 50 km) at close distances. It can be shown that the piercing points of these converted phases have offsets of up to 80 km so that they offer an independent possibility to image seismic structure in the Sea of Crete.

5 CONCLUSIONS

We employ receiver functions to derive a crust and upper-mantle model of the Hellenic subduction zone. Crustal thicknesses under central Crete are between 32 and 40 km. The negative amplitudes of *P–S* conversions from a boundary in this depth range at station SKD in western Crete and FODE in north-central Crete can be explained by reversed crust–mantle velocity contrast, caused by hydration and serpentinization of the forearc mantle. The crust thins to the south of Crete, beneath Gavdos island, where the Moho is observed at 26 km depth. In the central Aegean, at Naxos and Samos, the crustal thickness is between 25 an 28 km, implying only a moderate thinning of the crust since the inception of extension approximately 15 Ma. An anisotropic crustal structure is inferred beneath Santorini island. A boundary at approximately 25 km depth may represent the Moho of the Aegean subplate, which overlies a thinned remnant of the Cretan microcontinent where the bottom boundary (the Moho) is located at 32 km depth. The oceanic Moho of the subducting Hellenic slab can be traced from Gavdos to the volcanic arc (Santorini), with depth

increasing from 44 to 100 km. This boundary may continue to greater depth beneath Naxos, although the correlation is hampered by the lack of data in the Aegean Sea.

ACKNOWLEDGMENTS

GÜNTER BOCK

Günter Bock died on 2002 November 6 in an aeroplane crash in Luxembourg. He was on his way to a meeting of the Eifel Plume Project. Günter was born in 1944 in Paderborn/Westfalen and studied Geophysics at the University of München from 1965 to 1971, and received his PhD from the University of Karlsruhe in 1978. His dissertation was on 'Reservoir induced seismicity: models and observations'. From 1979 to 1983 he was a Research Fellow at the Australian National University in Canberra and from 1984 to 1992 Senior Lecturer at the University of New England in Armidale, Australia. Since 1992 he was Senior Research Scientist at the GeoForschungsZentrum (GFZ) Potsdam, Germany.

He was a truly broad seismologist with research interests in many fields, especially the global structure of the upper mantle, seismic anisotropy, and source mechanisms of shallow and deep earthquakes. Günter enjoyed travelling, but not only for field experiments to study the lithosphere in many parts of the world. He also spent much of his time in serving the scientific community by providing focal mechanisms of European earthquakes for the EMSC and as co-editor of the *Geophysical Journal International*. Many miss him not only as an unselfish colleague, but also as a friend in many happy times, including playing football. Günter left behind his wife, Gisela, and two sons, Mathis and Sebastian.

REFERENCES

Abers, G.A.,, 2000. Hydrated subducted crust at 100–250 km depth, *Earth planet. Sci. Lett.,* **176,** 323–330.

Angelier, J., Lybéris, Le Pichon, X., Barrier, E. & Huchon, P., 1982. The tectonic development of the Hellenic arc and the Sea of Crete: a synthesis, *Tectonophysics,* **86,** 159–196.

Avigad, D., Ziv, A. & Garfunkel, Z., 2001. Ductile and brittle shortening, extension-parallel folds and maintenance of crustal thickness in the central Aegean (Cyclades, Greece), *Tectonics,* **20,** 277–287.

Bock, G., Schurr, B. & Asch, G., 2000. High-resolution image of the oceanic Moho in the subducting Nazca Plate from *P–S* converted waves, *Geophys. Res. Lett.,* **27,** 3929–3932.

Bohnhoff, M., Makris, J., Papanikolaou, D. & Stavrakakis, G., 2001. Crustal investigation of the Hellenic subduction zone using wide aperture seismic data, *Tectonophysics,* **343,** 239–262.

Bostock, M.G., Hyndman, R.D., Rondeny, S. & Peacock, S.M., 2002. An inverted continental Moho and serpentinization of the forearc mantle, *Nature,* **417,** 536–538.

Cassidy, J.F., 1992. Numerical experiments in broadband receiver function analysis, *Bull. seism. Soc. Am.,* **82,** 1453–1474.

Engdahl, E.R., van der Hilst, R. & Buland, R., 1998. Global teleseismic earthquake relocation with improved travel times and procedures for depth determination, *Bull. seism. Soc. Am.,* **88,** 722–743.

Giese, P., Scheuber, E., Schilling, F., Schmitz, M. & Wigger, P., 1999. Crustal thickening processes in the Central Andes and the different natures of the Moho-discontinuity, *J. S. Am. Earth Sci.,* **12,** 201–220.

Hatzfeld, D. *et al.,* 2001. Shear wave anisotropy in the upper-mantle beneath the Aegean related to internal deformation, *J. geophys. Res.,* **106,** 30 737–30 753.

Helffrich, G., 2000. Topography of the transition zone seismic discontinuity, *Rev. Geophys.,* **38,** 141–158.

Hyndman, R.D. & Peacock, S.M., 2003. Serpentinization of the forearc mantle, *Earth planet. Sci. Lett.,* **212,** 417–432.

Jackson, J., 1994. Active tectonics in the Aegean region, *Ann. Rev. Earth planet. Sci.,* **22,** 239–271.

Jackson, J. & McKenzie, D., 1984. Active tectonics of the Alpine–Himalayan belt between western Turkey and Pakistan, *Geophys. J. R. astr. Soc.,* **77,** 185–264.

Jarrard, R.D., 1986. Relations among subduction parameters, *Rev. Geophys.,* **24,** 217–284.

Kastens, K., 1991. Rate of growth of the Mediterranean ridge accretionary complex, *Tectonophysics,* **199,** 25–50.

Kennett, B.L.N. & Engdahl, E.R., 1991. Travel times for global earthquake location and phase identification, *Geophys. J. Int.,* **105,** 429–465.

Kind, R. & Vinnik, L.P., 1988. The upper mantle discontinuities underneath the GRF array from *P*-to-*S* converted phases, *J. Geophys.,* **62,** 138–147.

Kind, R. *et al.,* 2002. Seismic images of the crust and upper mantle beneath Tibet: Evidence for Eurasian plate subduction, *Science,* **298,** 1219–1221.

Knapmeyer, M., 1999. Geometry of the Aegean Benioff zones, *Ann. Geofis.,* **42,** 27–38.

Knapmeyer, M. & Harjes, H.P., 2000. Imaging crustal discontinuities and the downgoing slab beneath western Crete, *Geophys. J. Int.,* **143,** 1–21.

Langston, C.A., 1977. Corvallis, Oregon, crustal and upper mantle structure from teleseismic *P* and *S* waves, *Bull. seism. Soc. Am.,* **67,** 713–724.

Le Pichon, X. & Angelier, J., 1979. The Hellenic arc and trench system: a key to the neotectonic evolution of the eastern Mediterranean area, *Tectonophysics,* **60,** 1–42.

Le Pichon, X., Chamot-Rooke, N., Lallemant, S., Noomen, R. & Veis, G., 1995. Geodetic determination of the kinematics of central Greece with respect to Europe: implications for eastern Mediterranean tectonics, *J. geophys. Res.,* **100,** 12 675–12 690.

Levin, V. & Park, J., 1997. *P–SH* conversions in a flat-layered medium with anisotropy of arbitrary orientation, *Geophys. J. Int.,* **131,** 253–266.

Li, X., Sobolev, S.V., Kind, R., Yuan, X. & Estabrook, Ch., 2000. A detailed receiver function image of the upper mantle discontinuities in the Japan subduction zone, *Earth planet. Sci. Lett.,* **183,** 527–541.

Li, X., Kind, R., Yuan, X., Sobolev, S.V., Hanka, W., Ramesh, D.S., Gu, Y. & Dziewonski, A.M., 2003. Seismic observation of narrow plumes in the oceanic upper mantle, *Geophys. Res. Lett.,* **30,** 10.1029/2002GL015411.

McClusky, S. *et al.,* 2000. Global Positioning system constraints on plate kinematics and dynamics in the eastern Mediterranean and Caucasus, *J. geophys. Res.,* **105,** 5695–5720.

McKenzie, D., 1972. Active tectonics in the Mediterranean region, *Geophys. J. R. astr. Soc.,* **30,** 109–185.

Makris, J., 1976. A dynamic model of the Hellenic arc deduced from geophysical data, *Tectonophysics,* **36,** 339–346.

Makropoulos, K.C. & Burton, P.W., 1984. Greek tectonics and seismicity, *Tectonophysics,* **106,** 275–304.

Owens, T.J., Zandt, G. & Taylor, S.R., 1984. Seismic evidence for an ancient rift beneath the Cumberland Plateau, Tennessee: a detailed analysis of broadband teleseismic *P* waveforms, *J. geophys. Res.,* **89,** 7783–7795.

Papanikolaou, D., Sakellariou, D. & Stoeckhert, B., 1999. A combined onshore/offshore drilling transect across the forearc of the retreating Hellenic subduction zone, *ICDP News.,* **1,** 22–24.

Papazachos, C., 1999. An alternative method for a reliable estimation of seismicity with an application in Greece and the surrounding area, *Bull. seism. Soc. Am.,* **89,** 111–119.

Papazachos, C.B. & Kiratzi, A.A., 1996. A detailed study of the active crustal deformation in the Aegean and surrounding area, *Tectonophysics,* **253,** 129–153.

Papazachos, B.C. & Nolet, G., 1997. *P* and *S* deep velocity structure of the Hellenic arc obtained by robust nonlinear inversion of travel times, *J. geophys. Res.,* **102,** 8349–8367.

Papazachos, B.C., Karakostas, V.G., Papazachos, C.B. & Scordilis, E.M., 2000. The geometry of the Wadati–Benioff zone and lithospheric kinematics in the Hellenic arc, *Tectonophysics,* **319,** 275–300.

Peacock, S.M., 1993. The importance of blueshist–eclogite dehydration reactions in subducting oceanic crust, *Bull. geol. Soc. Am.,* **105,** 684–694.

Priestley, K., Hatzfeld, D., Bock, G., Lyon.Caen, H., Kiratzi, A. & Makropoulos, K., 2000. Crustal velocity structure beneath the Aegean, *AGU 2000 Fall Meeting*.

Reilinger, R. *et al.,* 1997. Global positioning system measurements of present-day crustal movements in the Arabia–Africa–Eurasia plate collision zone, *J. geophys. Res.,* **102,** 9983–9999.

Spakman, W., Wortel, M.J.R. & Vlaar, N.J., 1988. The Hellenic subduction zone: a tomographic image and it geodynamic implications, *Geophys. Res. Lett.,* **15,** 60–63.

Ulmer, P. & Trommsdorff, V., 1995. Serpentine stability to mantle depths and subduction-related magmatism, *Science,* **268,** 858–861.

von Huene, R., 1997. Mediterannean ridge structure: results from IMERSE, *EOS, Trans. Am. geophys. Un.,* **78,** 155.

Wortel, M.J.R., Goes, S.D.B. & Spakman, W., 1990. Structure and seismicity of the Aegean subduction zone, *TerraNova,* **2,** 554–562.

Yuan, X., Ni, J., Kind, R., Mechie, J. & Sandvol, E., 1997. Lithospheric and upper mantle structure of southern Tibet from a seismological passive source experiment, *J. geophys. Res.,* **102,** 27 491–27 500.

Yuan, X. *et al.,* 2000. New constraints on subduction and collision processes in the Central Andes from *P*-to-*S* converted seismic phases, *Nature,* **408,** 958–961.

Yuan, X., Sobolev, S.V. & Kind, R., 2002. Moho topography in the central Andes and its geodynamic implication, *Earth planet. Sci. Lett.,* **199,** 389–402.